available at www.sciencedirect.com
journal homepage: euoncology.europeanurology.com

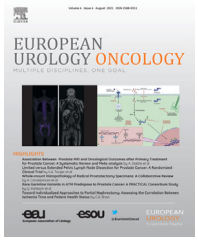

European Association of Urology

A Prospective Comparison of ^{18}F-prostate-specific Membrane Antigen-1007 Positron Emission Tomography Computed Tomography, Whole-body 1.5 T Magnetic Resonance Imaging with Diffusion-weighted Imaging, and Single-photon Emission Computed Tomography/Computed Tomography with Traditional Imaging in Primary Distant Metastasis Staging of Prostate Cancer (PROSTAGE)

Mikael Anttinen[a,*], *Otto Ettala*[a], *Simona Malaspina*[b], *Ivan Jambor*[c,d], *Minna Sandell*[c], *Sami Kajander*[b], *Irina Rinta-Kiikka*[e], *Jukka Schildt*[f], *Ekaterina Saukko*[c], *Pentti Rautio*[g], *Kirsi L. Timonen*[h], *Tuomas Matikainen*[a], *Tommi Noponen*[i], *Jani Saunavaara*[i], *Eliisa Löyttyniemi*[j], *Pekka Taimen*[k], *Jukka Kemppainen*[b], *Peter B. Dean*[c], *Roberto Blanco Sequeiros*[c], *Hannu J. Aronen*[c], *Marko Seppänen*[l], *Peter J. Boström*[a]

[a] *Department of Urology, University of Turku and Turku University Hospital, Turku, Finland;* [b] *Turku PET Centre, University of Turku and Turku University Hospital, Turku, Finland;* [c] *Department of Diagnostic Radiology, University of Turku and Turku University Hospital, Turku, Finland;* [d] *Department of Radiology, Icahn School of Medicine at Mount Sinai, New York, NY, USA;* [e] *Department of Radiology, Tampere University and Tampere University Hospital, Tampere, Finland;* [f] *Department of Clinical Physiology and Nuclear Medicine, University of Helsinki and Helsinki University Hospital, Helsinki, Finland;* [g] *Department of Clinical Physiology, North Karelia Central Hospital, Joensuu, Finland;* [h] *Department of Clinical Physiology and Nuclear Medicine, Central Hospital of Central Finland, Jyväskylä, Finland;* [i] *Department of Medical Physics and Nuclear Medicine, University of Turku and Turku University Hospital, Turku, Finland;* [j] *Department of Biostatistics, University of Turku, Turku, Finland;* [k] *Institute of Biomedicine, University of Turku and Department of Pathology, Turku University Hospital, Turku, Finland;* [l] *Department of Clinical Physiology, Nuclear Medicine and Turku PET Centre, University of Turku and Turku University Hospital, Turku, Finland*

Article info

Article history:
Received 6 May 2020
Received in revised form
8 June 2020
Accepted June 29, 2020

Associate Editor:
Gianluca Giannarini

Keywords:
Advanced imaging
Conventional imaging

Abstract

Background: Computed tomography (CT) and bone scintigraphy (BS) are the imaging modalities currently used for distant metastasis staging of prostate cancer (PCa).

Objective: To compare standard staging modalities with newer and potentially more accurate imaging modalities.

Design, setting, and participants: This prospective, single-centre trial (NCT03537391) enrolled 80 patients with newly diagnosed high-risk PCa (International Society of Urological Pathology grade group $\geq$3 and/or prostate-specific antigen [PSA] $\geq$20 and/or cT $\geq$ T3; March 2018–June 2019) to undergo primary metastasis staging with two standard and three advanced imaging modalities.

Outcome measurements and statistical analysis: The participants underwent the following five imaging examinations within 2 wk of enrolment and without a

* Corresponding author. Department of Urology, Turku University Hospital, University of Turku, Kiinamyllynkatu 4-8, 20521 Turku, Finland. Tel.: +358-2-3133650; Fax: +358-2-3132284.
E-mail addresses: mhjant@utu.fi, mikael.anttinen@tyks.fi (M. Anttinen).

https://doi.org/10.1016/j.euo.2020.06.012

Distant metastasis
^{18}F-prostate-specific membrane antigen-1007
Primary metastasis staging
Prostate cancer
Prostate-specific membrane antigen positron emission tomography/computed tomography
Single-photon emission computed tomography/computed tomography
Whole-body magnetic resonance imaging

prespecified sequence: BS, CT, ^{99m}Tc-hydroxymethylene diphosphonate (^{99m}Tc-HMDP) single-photon emission computed tomography (SPECT)-CT, 1.5 T whole-body magnetic resonance imaging (WBMRI) using diffusion-weighted imaging, and ^{18}F-prostate-specific membrane antigen-1007 (^{18}F-PSMA-1007) positron emission tomography(PET)-CT. Each modality was reviewed by two independent experts blinded to the results of the prior studies, who classified lesions as benign, equivocal, or malignant. Pessimistic and optimistic analyses were performed to resolve each equivocal diagnosis. The reference standard diagnosis was defined using all available information accrued during at least 12 mo of clinical follow-up. Patients with equivocal reference standard diagnoses underwent MRI and/or CT to search for the development of anatomical correspondence. PSMA PET-avid lesions without histopathological verification were rated to be malignant only if there was a corresponding anatomical finding suspicious for malignancy at the primary or follow-up imaging.

Results and limitations: Seventy-nine men underwent all imaging modalities except for one case of interrupted MRI. The median interval per patient between the first and the last imaging study was 8 d (interquartile range [IQR]: 6–9). The mean age was 70 yr (standard deviation: 7) and median PSA 12 ng/mL (IQR:7–23). The median follow-up was 435 d (IQR: 378–557). Metastatic disease was detected in 20 (25%) patients. The imaging modality ^{18}F-PSMA-1007 PET-CT had superior sensitivity and highest inter-reader agreement. The area under the receiver-operating characteristic curve (AUC) values for bone metastasis detection with PSMA PET-CT were 0.90 (95% confidence interval [CI]: 0.85–0.95) and 0.91 (95% CI: 0.87–0.96) for readers 1 and 2, respectively, while the AUC values for BS, CT, SPECT-CT, and WBMRI were 0.71 (95% CI: 0.58–0.84) and 0.8 (95% CI: 0.67–0.92), 0.53 (95% CI: 0.39–0.67) and 0.66 (95% CI: 0.54–0.77), 0.77 (95% CI: 0.65–0.89) and 0.75 (95% CI: 0.62–0.88), and 0.85 (95% CI: 0.74–0.96) and 0.67 (95% CI: 0.54–0.80), respectively, for the other four pairs of readers. The imaging method ^{18}F-PSMA-1007 PET-CT detected metastatic disease in 11/20 patients in whom standard imaging was negative and influenced clinical decision making in 14/79 (18%) patients. In 12/79 cases, false positive bone disease was reported only by PSMA PET-CT. Limitations included a nonrandomised study setting and few histopathologically validated suspicious lesions.

Conclusions: Despite the risk of false positive bone lesions, ^{18}F-PSMA-1007 PET-CT outperformed all other imaging methods studied for the detection of primary distant metastasis in high-risk PCa.

Patient summary: In this report, we compared the diagnostic performance of conventional and advanced imaging. It was found that ^{18}F-prostate-specific membrane antigen-1007 positron emission tomography/computed tomography (^{18}F-PSMA-1007 PET-CT) was superior to the other imaging modalities studied for the detection of distant metastasis at the time of initial diagnosis of high-risk prostate cancer. PSMA PET-CT also appears to detect some nonmetastatic bone lesions.

1. Introduction

Many men diagnosed and treated for localised prostate cancer (PCa) have distant recurrence, indicating that metastatic spread was present at the time of initial diagnosis [1]. Tumour spread to soft tissues, especially lymph nodes (LNs), is traditionally evaluated with computed tomography (CT) of the abdomen and pelvis or with pelvic magnetic resonance imaging (MRI), which have limited sensitivity [2,3]. Search for bone metastases commonly uses methodologies with limited accuracy, such as bone scintigraphy (BS) and CT [4,5].

Prostate-specific membrane antigen (PSMA) positron emission tomography (PET) has emerged as a promising diagnostic tool for PCa staging [6], and a multicentre trial recently reported superiority of ^{68}Ga-PSMA-11 PET-CT over conventional imaging in primary staging of high-risk PCa [7]. However, several questions remain unanswered, including superiority of PSMA PET-CT over other novel imaging modalities, particularly whole-body MRI (WBMRI). WBMRI

with diffusion-weighted imaging (DWI) is an effective method for overall staging in PCa, showing improved detection of bone metastases compared with traditional imaging [5]. DWI can detect metastases in normal-sized LNs and early intramedullary bone metastases before the appearance of cortical destruction or reactive processes [8,9]. Furthermore, the optimal tracer for PSMA PET imaging has not been determined. The novel ^{18}F-labeled PET tracers DCFPyL and PSMA-1007 are promising PSMA-targeting ligands [10,11]. The half-life of ^{18}F-PSMA is longer than that of ^{68}Ga-PSMA; ^{18}F-PSMA is cyclotron produced, enabling centralised production in larger quantities and long-distance transport, providing a more practical option for PCa imaging [12]. Finally, there are only limited validation data on PSMA-avid lesions lacking anatomic correspondence [13].

We have previously demonstrated the superior diagnostic accuracy of ^{18}F-NaF PET-CT, WBMRI, and ^{99m}Tc-hydroxymethylene diphosphonate (^{99m}Tc-HMDP) single-photon emission computed tomography (SPECT)-CT over BS for the detection of PCa bone metastases in a prospective setting (SKELETA trial) [5]. These findings needed further validation as there were few (n = 27) PCa patients, there were no soft tissue assessment, and PSMA PET-CT was not included. The rationale for the present trial was to find the most appropriate initial staging modality for high-risk PCa.

2. Patients and methods

2.1. Study design

This investigator initiated, nonrandomised, prospective, single-institutional trial (ClinicalTrials.gov NCT03537391) compared the diagnostic accuracy of advanced imaging modalities with that of traditional ones in primary staging of men with high-risk PCa. We report the results of distant metastasis staging from this multimodality research project. For clarity, the T staging and N staging are being reported separately. The trial was approved by the local ethics committee, and written informed consent was obtained from all participants. The study outline is illustrated in Figure 1.

2.2. Participants and study procedures

Between March 2018 and June 2019, men (n = 80) with primary histopathologically confirmed high-risk PCa were prospectively enrolled. Patients aged at least 18 yr were eligible if they met at least one of the following criteria: (1) International Society of Urological Pathology (ISUP) grade group ≥3, (2) prostate-specific antigen (PSA) ≥20 ng/mL, and (3) clinical tumour stage ≥3a. Exclusion criteria included any previous PCa imaging for metastasis staging, PCa treatment before enrolment, and contraindications for MRI (pacemaker, intracranial clips, etc.). Each imaging study was arranged within 2 wk after enrolment without a prespecified sequence. Administration of androgen deprivation therapy (ADT) at enrolment was permitted if necessary for symptomatic very-high-risk PCa patients.

After consenting, participants were referred for metastasis staging with all the following imaging modalities:

1 Standard imaging: ^{99m}Tc-HMDP planar BS and contrast-enhanced CT of the thorax, abdomen, and pelvis
2 Imaging under evaluation: ^{18}F-PSMA-1007 PET-CT, WBMRI including DWI, and ^{99m}Tc-HMDP SPECT-CT

A detailed description of each imaging modality is given in the Supplementary material. The patients were followed for at least 12 mo and follow-up imaging was performed, if necessary, to validate equivocal imaging findings.

2.3. Image reporting

Each imaging modality was independently double read by two experienced modality-based experts, from a group of six nuclear medicine physicians and four radiologists. Experience of the expert

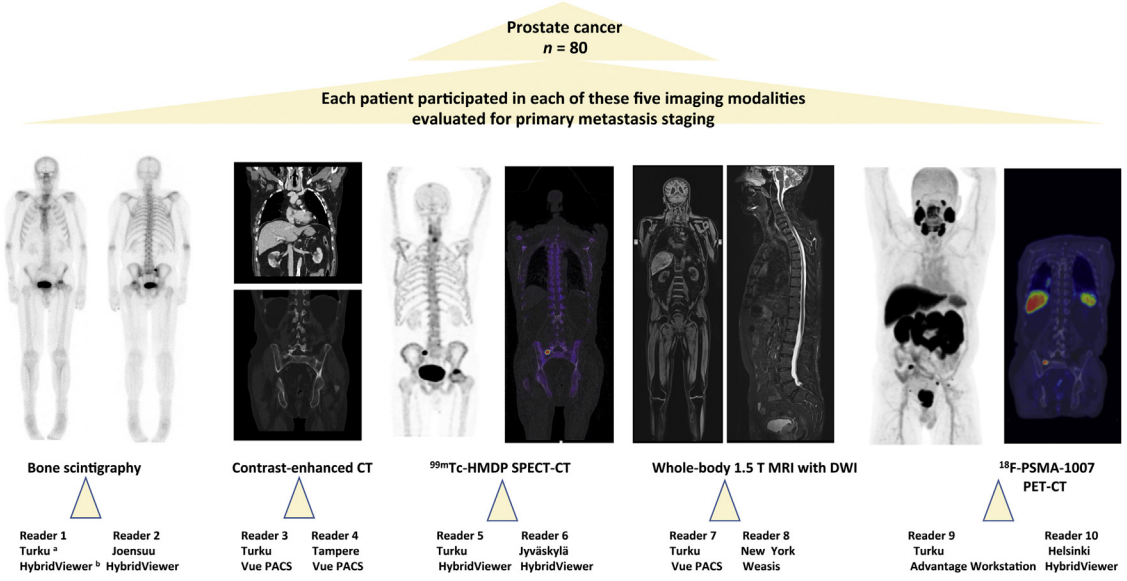

Fig. 1 – Study outline. CT = computed tomography; DWI = diffusion-weighted imaging; HMDP = hydroxymethylene diphosphonate; MRI = magnetic resonance imaging; PET = positron emission tomography; PSMA = prostate-specific membrane antigen; SPECT = single-photon emission computed tomography. [a] The location (city) of the reader. [b] The software used for image interpretation: HybridViewer (version 2.6 P; Hermes Medical Solutions, Stockholm, Sweden), Advantage Workstation (version 4.7; GE Healthcare, Buc, France), Weasis Medical Viewer (version 3.5.3; University of Geneva, Geneva, Switzerland), and Vue PACS (version 12.2.0.1007; Carestream Health Inc., Rochester, NY, USA).

readers is shown in Supplementary Table S1 . The readers were blinded to the other imaging modalities and informed that the patients presented with high-risk PCa. The lesions were interpreted according to clinical expertise complying with the current guidelines and reported as malignant, equivocal, or benign [2,14]. The software used for image interpretations are shown in Figure 1. Study data were collected and managed using a REDCap electronic data capture tool [15]. A detailed description of the interpretation of metastatic lesions is given in the Supplementary material.

The nature of each reported lesion was defined based on the regularly organised consensus meetings by a multidisciplinary team, including at least one uro-oncologist, one uropathologist, two radiologists (CT and MRI specialists), and one nuclear medicine physician. The examination results from all primary and follow-up imaging modalities, and clinical follow-up data (including PSA kinetics and, when available, histopathological specimens) were utilised to determine the reference standard diagnosis [7,16–18] for each lesion. The lesions reported from each modality were rated according to this reference standard diagnosis, which was determined by consensus as either benign or malignant. Equivocal findings reported by the investigational readers were all reclassified as malignant or benign according to a pessimistic or an optimistic analysis, respectively.

PSMA PET-avid lesions lacking histopathological verification were rated as malignant only if there was a corresponding anatomical finding suspicious for malignancy at primary or follow-up MRI and/or CT (Supplementary material). If there were no typical benign or malignant finding on MRI/CT within lesions associated with a tracer uptake, excluding normal physiological uptake areas, follow-up imaging was used to identify possible development of anatomical correspondence using MRI and/or CT from the region of interest. If follow-up imaging did not reveal anatomical correspondence, the lesion was considered nonmalignant (false positive).

The bone and soft tissue findings were compared at the patient, region, and lesion levels. The regions were divided into three categories according to the eighth edition of UICC 2009 tumour node metastasis (TNM) classification for PCa [19].

2.4. Outcomes

The primary outcome was detection of bone metastasis. The secondary outcomes included detection of soft tissue metastasis and the effect of staging on clinical treatment decision making.

2.5. Statistical analysis

This study was designed to demonstrate a possibly improved diagnostic performance of three advanced imaging modalities compared with two traditional ones in the primary staging of high-risk PCa. The primary outcome measurement was the diagnostic accuracy assessed by the area under the receiver-operating characteristic curve (AUC) values of bone metastasis detection in the pessimistic analysis (equivocal lesions classified as malignant).

The sample size estimation was based on our previously published pilot trial SKELETA [5], where AUC values for PET-CT and BS were 0.91 and 0.72, respectively. We estimated that for the detection of a 0.19 difference in the AUC value using a two-tailed test with a power of 80% at a significance level of 0.05 in a 2:1 ratio of sample sizes in negative/positive groups, 48 cases and 24 positive cases were required. Accounting for possible dropouts, the recruitment goal was 80 patients.

The sensitivity, specificity, and accuracy values are reported with a 95% confidence interval (CI) and compared between modalities with Fisher's exact test. The inter-reader agreement at the patient level was defined using Cohen's kappa (95% CI). The AUC values were calculated using the trapezoid rule. The AUC values in the pessimistic analysis at the region level (bone) were calculated and compared using a method by Hanley and McNeil [20]. The analysis was performed using logistic regression. All p values of <0.05 were considered statistically significant. All statistical analyses were performed with the SAS system (version 9.4 for Windows; SAS Institute Inc., Cary, NC, USA).

3. Results

Eighty patients were enrolled, and 79 patients completed the study. The study flow chart is presented in Figure 2. Except for one case of interrupted MRI due to unexpected claustrophobia, all patients were studied with all imaging modalities, resulting in 394 imaging examinations and 788 interpretations. The median interval per patient between the first and the last imaging study was 8 d (interquartile range [IQR]: 6–9). The median follow-up period per patient was 435 d (IQR: 378–557).

The clinical characteristics are presented in Table 1. Of 79 patients, 20 had metastatic disease. Of these patients, nine had bone, four had extraregional nodal, four had bone and extraregional nodal, and three had bone, extraregional nodal, and visceral metastases (all pulmonary metastases). Four patients (5%) each had a significant additional imaging finding detected by PSMA PET-CT, CT, and MRI (neck paraganglioma, renal carcinoma, brain tumour, and bladder carcinoma). There were no PSMA-negative bone metastases, but in one patient a PSMA-negative extraregional LN disease (M1a) was detected only with MRI.

In one case, there was a PSMA-avid (maximum standardised uptake value [SUVmax] 3.0) sclerotic lesion on the right scapula. CT-guided biopsy from the lesion revealed fibrous dysplasia. The same patient also had PSMA-avid lesions without anatomical correspondence in the ribs (SUVmax 2.3, 2.9, and 2.5) and femur (SUVmax 3), all considered benign. In another patient, a PSMA-avid (SUVmax 6.5), round, 11-mm LN in the left axilla, the largest of several similar LNs, was confirmed to be reactive through ultrasound-guided biopsy.

Primary external beam radiotherapy was given to 37/79 (47%) patients. In 11 (30%) cases, the clinical target volume in radiotherapy was changed after PSMA PET-CT. Robot-assisted laparoscopic prostatectomy was performed in 22/79 (28%) patients. Of these 22 surgical patients, pelvic lymphadenectomy was performed in 17. In two of the 22 (9%) patients, advanced imaging affected the surgical approach or the adjuvant treatment. Surgery was considered curative in 17/22 cases based on a 3-mo PSA level of <0.1 ng/mL (of which eight patients had a PSA level of <0.006; Supplementary Fig. S1). Two (3%) patients underwent MRI-guided transurethral ultrasound ablation. In five (6%) cases, ADT was administered at enrolment due to symptomatic high-volume metastatic disease, and four of these patients underwent early chemohormonal therapy. Of 79 (16%) patients, 13 were treated only by continuous ADT. In two (3%) patients, ADT was initiated due to metastatic disease detected only by PSMA PET-CT.

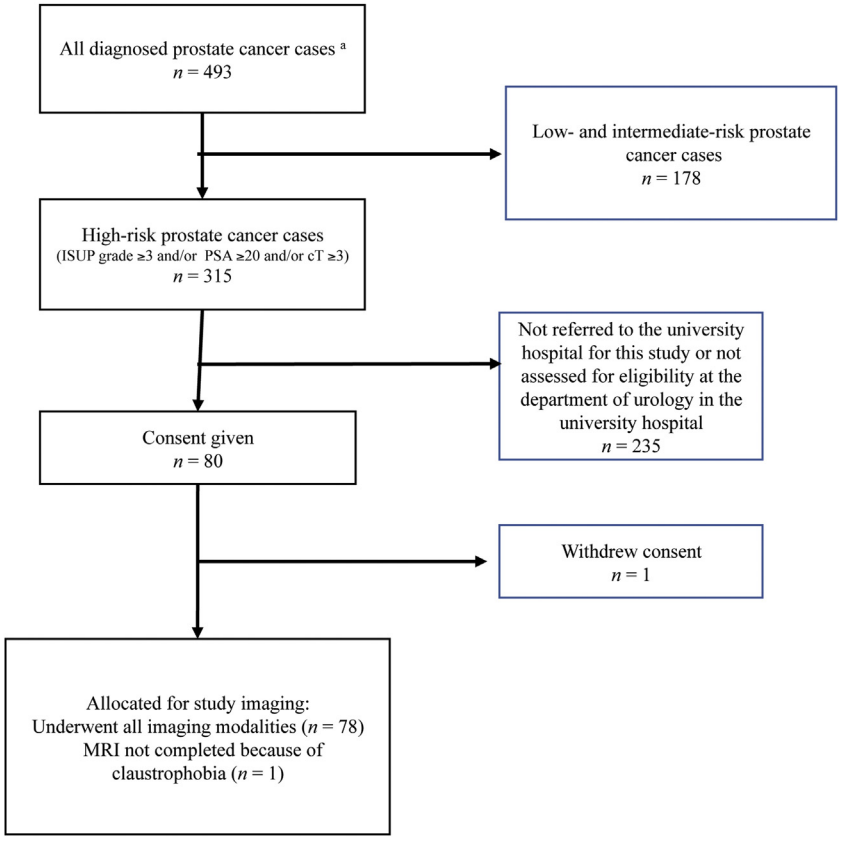

Fig. 2 – Study flow chart. ISUP = International Society of Urological Pathology; MRI = magnetic resonance imaging; PSA = prostate-specific antigen. [a] All men in the hospital district of Southwest Finland had a new diagnosis of prostate cancer during the period from March 2018 through May 2019. Study patients were identified for this study by the Department of Urology at the Turku University Hospital.

Table 1 – Patient demographics, disease characteristics, and primary treatment methods.

Age (yr), mean (SD)	70 (7)
PSA (ng/mL), median (IQR [range])	12 (7–23 [3–2000])
Clinical T stage, *n* (%)[a]	
cT1	7 (9)
cT2	38 (48)
cT3	27 (34)
cT4	8 (10)
Biopsy ISUP grade group, *n* (%)	
1[b]	3 (4)
2	1 (1)
3	29 (36)
4	13 (16)
5	34 (42)
Primary treatment methods, *n* (%)[c]	
RALP	5 (6)
RALP + lymphadenectomy	17 (21)
EBRT	38 (48)
TULSA	2 (3)
ADT	17 (21)
Watchful waiting	1 (1)

ADT = androgen deprivation therapy with (*n* = 4) or without (*n* = 13) early chemotherapy with docetaxel; EBRT = external beam radiotherapy with (*n* = 37) or without (*n* = 1) ADT; IQR = interquartile range; ISUP = International Society of Urological Pathology; PSA = prostate specific antigen; RALP = robot-assisted laparoscopic prostatectomy; SD = standard deviation; TULSA = transurethral ultrasound ablation of the prostate.

All patients were Caucasians and presented with good performance status at the time of enrolment (Eastern Cooperative Oncology Group Performance status 0–1).

[a] Clinical T stage was determined based on transrectal ultrasound and digital rectal examination before any imaging.

[b] All patients with ISUP grade group 1 had PSA > 20 ng/mL.

[c] In two cases, palliative transurethral resection of the prostate was performed due to bladder outlet obstruction prior to EBRT, and one case underwent palliative TULSA combined with ADT.

Table 2 – Sensitivity, specificity, and accuracy of both readers of each imaging modality in pessimistic and optimistic analysis at the patient level.

Imaging modality and reader	Pessimistic analysis			Optimistic analysis		
	Sensitivity (95% CI)	Specificity (95% CI)	Accuracy (95% CI)	Sensitivity (95% CI)	Specificity (95% CI)	Accuracy (95% CI)
CT 1	0.57 (0.36–0.78)[a,b]	0.33 (0.21–0.45)[a,b]	0.39 (0.27–0.52)[a,b]	0.43 (0.22–0.64)[a,b]	0.79 (0.69–0.90)	0.70 (0.58–0.81)[b]
CT 2	0.43 (0.22–0.64)[a,b]	0.95 (0.89–1.01)[a,b]	0.81 (0.71–0.91)	0.33 (0.13–0.53)[a,b]	0.98 (0.95–1.02)[b]	0.81 (0.71–0.91)
SPECT-CT 1	0.67 (0.47–0.87)[b]	0.74 (0.63–0.85)	0.72 (0.61–0.84)	0.52 (0.31–0.73)[a,b]	0.97 (0.92–1.01)[b]	0.85 (0.76–0.94)
SPECT-CT 2	0.57 (0.36–0.78)[a,b]	0.86 (0.77–0.95)	0.78 (0.68–0.84)[b]	0.33 (0.13–0.53)[a,b]	0.98 (0.95–1.01)[b]	0.81 (0.71–0.94)
WBMRI + DWI 1	0.67 (0.47–0.87)[b]	0.80 (0.70–0.91)	0.77 (0.66–0.88)	0.67 (0.47–0.87)	0.96 (0.91–1.01)[b]	0.88 (0.80–0.97)
WBMRI + DWI 2	0.52 (0.31–0.74)[a,b]	0.82 (0.72–0.92)	0.74 (0.63–0.86)	0.43 (0.22–0.64)[a,b]	0.96 (0.91–1.01)[b]	0.82 (0.72–0.92)
PSMA PET-CT 1	0.90 (0.78–1.00)	0.76 (0.65–0.87)	0.80 (0.69–0.90)	0.86 (0.71–1.00)	0.90 (0.82–0.97)	0.89 (0.80–0.97)
PSMA PET-CT 2	0.95 (0.86–1.00)	0.79 (0.69–0.90)	0.84 (0.74–0.93)	0.95 (0.86–1.00)	0.81 (0.71–0.91)	0.85 (0.76–0.94)

BS = bone scintigraphy; CI = confidence interval; CT = computed tomography; DWI = diffusion-weighted imaging; PET = positron emission tomography; PSMA = prostate-specific membrane antigen; SPECT = single-photon emission computed tomography; WBMRI = whole-body magnetic resonance imaging.
Planar BS was excluded from the patient-level analysis due to its inability to assess soft tissues.
Metastatic disease was revealed by standard imaging (combination of BS and CT), SPECT-CT, WBMRI, and PSMA PET-CT in nine, 11, 13, and 19 of 20 patients, respectively.
The exact *p* values are presented in Supplementary Table S2.
[a] Statistically significant difference ($p < 0.05$) compared with PSMA PET-CT 1.
[b] Statistically significant difference ($p < 0.05$) compared with PSMA PET-CT 2.

Altogether 1137 malignant and 444 equivocal lesions were identified. The reported equivocal lesions were distributed among modalities as follows: BS 41 (reader 1: $n = 18$, and reader 2: $n = 23$), CT 208 (183 and 25), SPECT-CT 76 (34 and 42), MRI 85 (47 and 38), and PSMA PET-CT 34 (21 and 13). All 1581 lesions were consensus read, resulting in 212 lesions considered as malignant (the reference standard diagnosis): 129 bone, 53 extraregional LN, and 30 visceral.

The results of the analyses at patient level are shown in Table 2 and Supplementary Table S2. PSMA PET-CT detected metastatic disease in 11 of 20 patients in whom standard imaging (combination of BS and CT) was negative and in six of 20 patients in whom all other imaging modalities were negative (Supplementary Fig. S2). The inter-reader agreement values (kappa) in the pessimistic analysis at the patient level were 0.56 (95% CI: 0.34–0.77), 0.02 (95% CI: 0.11–0.14), 0.46 (95% CI: 0.26–0.66), 0.34 (95% CI: 0.11–0.56), and 0.82 (95% CI: 0.69–0.95) for BS, CT, SPECT-CT, WBMRI, and PSMA PET-CT, respectively.

The results of the analyses of the bone and soft tissue regions are shown in Table 3, and Supplementary Tables S3 and S4. At the region level (bone), PSMA PET-CT was significantly more sensitive than other imaging modalities. Notably, PSMA PET-CT was superior to the other imaging modalities regarding the AUC values (reader 1: 0.90 [95% CI: 0.85–0.95], reader 2: 0.91 [95% CI: 0.87–0.96]) in the pessimistic analysis at region level (bone) and met our primary endpoint (Supplementary Table S5).

Table 3 – Sensitivity, specificity, and accuracy of both readers of each imaging modality in pessimistic and optimistic analysis at the region level (bone).

Imaging modality and reader	Pessimistic analysis			Optimistic analysis		
	Sensitivity (95% CI)	Specificity (95% CI)	Accuracy (95% CI)	Sensitivity (95% CI)	Specificity (95% CI)	Accuracy (95% CI)
Bone scintigraphy 1	0.50 (0.26–0.75)[a,b]	0.89 (0.81–0.97)	0.81 (0.71–0.91)	0.38 (0.14–0.61)[a,b]	1.00 (1.00–1.00)[a,b]	0.87 (0.79–0.96)
Bone scintigraphy 2	0.69 (0.46–0.91)[a,b]	0.86 (0.77–0.94)	0.82 (0.73–0.92)	0.44 (0.19–0.68)[a,b]	1.00 (1.00–1.00)[a,b]	0.89 (0.81–0.96)
CT 1	0.56 (0.32–0.81)[a,b]	0.49 (0.37–0.62)[a,b]	0.51 (0.38–0.63)[a,b]	0.31 (0.09–0.54)[a,b]	0.87 (0.79–0.96)	0.76 (0.65–0.87)[a]
CT 2	0.25 (0.04–0.46)[a,b]	1.00 (1.00–1.00)[a,b]	0.85 (0.76–0.94)	0.25 (0.04–0.46)[a,b]	1.00 (1.00–1.00)[a,b]	0.85 (0.76–0.94)
SPECT-CT 1	0.69 (0.46–0.91)[a,b]	0.79 (0.69–0.89)	0.77 (0.67–0.88)	0.63 (0.39–0.86)[b]	0.97 (0.92–1.02)[b]	0.90 (0.82–0.97)
SPECT-CT 2	0.63 (0.39–0.86) [a,b]	0.87 (0.79–0.96)	0.82 (0.73–0.92)	0.44 (0.19–0.68) [a,b]	0.98 (0.95–1.01)[b]	0.87 (0.79–0.96)
WBMRI + DWI 1	0.69 (0.46–0.91)[a,b]	0.88 (0.81–0.97)	0.84 (0.75–0.94)	0.62 (0.39–0.86)[b]	0.98 (0.95–1.02)[b]	0.91 (0.84–0.98)
WBMRI + DWI 2	0.44 (0.19–0.69)[a,b]	0.90 (0.83–0.98)	0.81 (0.71–0.90)	0.44 (0.19–0.68)[a,b]	0.97 (0.92–1.01)[b]	0.86 (0.77–0.94)
PSMA PET-CT 1	1.00 (1.00–1.00)	0.79 (0.69–0.89)	0.84 (0.74–0.93)	0.94 (0.82–1.00)	0.90 (0.83–0.98)	0.91 (0.84–0.98)
PSMA PET-CT 2	1.00 (1.00–1.00)	0.83 (0.73–0.92)	0.86 (0.78–0.95)	1.00 (1.00–1.00)	0.90 (0.73–0.92)	0.86 (0.77–0.95)

CI = confidence interval; CT = computed tomography; DWI = diffusion-weighted imaging; PET = positron emission tomography; PSMA = prostate-specific membrane antigen; SPECT = single-photon emission computed tomography; WBMRI = whole-body magnetic resonance imaging.
The exact *p* values are presented in Supplementary Table S3.
[a] Statistically significant difference ($p < 0.05$) compared with PSMA PET-CT reader 1.
[b] Statistically significant difference ($p < 0.05$) compared with PSMA PET-CT reader 2.

Table 4 – The total number of lesions reported by both readers of each imaging modality and their concordance with the reference standard diagnosis at lesion level.

Imaging modality and reader number	Number of positive lesions reported	Number of true positive lesions	Detection rate of true positive lesions (%)	Number of false positive lesions	Number of false negative lesions	Number of equivocal lesions reported	Ratio of equivocal to all detected lesions (%)
BS 1	45	41	19	4	88	18	29
BS 2	57	51	24	6	78	23	29
CT 1	158	106	50	52	106	183	54
CT 2	82	74	35	8	138	25	23
SPECT-CT 1	106	99	47	7	113	34	24
SPECT-CT 2	76	67	32	9	145	42	36
WBMRI + DWI 1	95	88	42	7	124	47	33
WBMRI + DWI 2	131	78	37	53	134	38	22
PSMA PET-CT 1	205	183	86	22	29	21	9
PSMA PET-CT 2	182	152	72	30	60	13	7

BS = bone scintigraphy; CT = computed tomography; DWI = diffusion-weighted imaging; PET = positron emission tomography; PSMA = prostate-specific membrane antigen; SPECT = single-photon emission computed tomography; WBMRI = whole-body magnetic resonance imaging.
There were 212 malignant lesions (reference standard diagnoses) in the patient cohort, of which 129 were bone and 83 soft tissue lesions.

The number of all malignant and equivocal lesions reported by each reader and their concordance with the reference standard diagnosis are shown in Table 4. The total numbers of false positive lesions were 22 for PET reader 1 and 30 for PET reader 2. Supplementary Figures S3 and S4 demonstrate the SUVmax values of all reported malignant lesions for PSMA PET readers 1 and 2, respectively. The mean SUVmax values of all true positive (Supplementary Fig. S5) and false positive (Supplementary Fig. S6) lesions were 10.5 (range: 2.3–55.4) and 5.4 (range: 2.8–10.5), respectively. There were six and 12 false positive metastatic patients according to PET readers 1 and 2, respectively. Clinicopathological characteristics including all follow-up imaging and validation data are presented for both true positive (Supplementary Table S6) and false positive (Supplementary Table S7) PSMA PET lesions in detail.

4. Discussion

Our study design with prospective head-to-head comparison between the standard and advanced imaging modalities combined with extended follow-up provided detailed image-based characterisation and reliable validation of the metastatic lesions. In this study, 25% of the patients had metastatic disease and PSMA PET-CT detected 95% of these cases. PSMA PET-CT detected metastatic disease in 14% of the patients when standard imaging modalities were negative. PSMA PET-CT had superior sensitivity for detection of distant metastasis. However, 15% of the patients had false positive PSMA-PET findings at the patient level. Our strict requirement for anatomical correspondence of PSMA-avid lesions might underestimate the specificity of PSMA PET, a highly sensitive tool for detecting PCa metastases. In most of the cases, false positive PSMA PET findings were related to moderately increased bone uptake without any corresponding anatomical findings in primary or follow-up imaging. False positive uptake is most commonly caused by fractures and degenerative joint disease, and rarely by fibrous dysplasia (as in one of our cases), Paget's disease of the bone, and haemangiomas [13].

CT and BS have been the methods of choice for metastasis staging in newly diagnosed PCa [2]. Reliable exclusion of metastases in higher-risk cases is paramount since local radical therapy cannot achieve cure in the presence of distant metastases and may instead expose patients to treatment-related adverse effects without any therapeutic benefit. Few trials have demonstrated a survival benefit from local radical therapy in patients with low-volume metastatic disease [21].

As our results suggest, ^{18}F-PSMA-1007 PET-CT increases the detection of metastatic disease, mostly low-volume metastatic disease. The ultimate benefit of earlier metastasis detection upon prognosis, patient management, and survival has yet to be established. Despite this uncertainty, the recognition of oligometastatic disease using imaging modalities with higher sensitivity enables specific therapy of these metastases, which may postpone the need for debilitating systemic therapy and delay or even arrest metastatic progression [22–24]. In 14/79 (18%) of our patients, ^{18}F-PSMA-1007 PET-CT influenced clinical decision making.

One limitation of this trial is the nonrandomised trial setting. Accumulating evidence suggests that PSMA PET has a significant impact on treatment decision making [7,25], but additional evidence supporting the oncological benefit of detecting metastatic disease earlier by improved imaging is still needed. The main rationale for this study was to determine the most accurate imaging modality for metastasis staging of high-risk PCa in a prospective setting. Such data were lacking prior to this multimodality research project. There is encouraging evidence of improved metastasis detection with ^{68}Ga-PSMA-11 PET-CT over conventional imaging in patients with high-risk PCa; however, WBMRI was not included in these trials [7,25]. Further, the widespread utilisation of ^{68}Ga-PSMA-11 is challenging due to production capacity and nuclear decay properties. The novel ^{18}F-PSMA-1007

tracer could overcome these limitations [12]. The characterisation and validation of the novel ^{18}F-PSMA-1007-radiotracer, and its superiority to conventional imaging on metastasis staging, in which available data are limited, were among the objectives of this study, in preparation for further trials.

The lack of histopathologically verified distant metastatic lesions is an inherent limitation in studies where advanced and more sensitive imaging modalities such as PSMA PET-CT are likely to identify smaller lesions, some of which lack a corresponding morphological lesion necessary for successful image-guided biopsy [26]. In order to manage challenges of PSMA PET-avid lesions in the absence of histological verification, we chose strict validation criteria, that is, only PSMA PET-avid lesions with anatomical correspondence were considered true positive. Using these strict criteria, we may have classified some truly positive lesions as negative. Our results compare favourably with a recent multi-institutional study [7]. Using strict validation criteria, they detected distant metastases in 18/300 (6%) compared with 20/79 (25%) cases in our study.

Initiation of ADT for symptomatic very-high-risk patients at enrolment could be regarded as a minor limitation; however, all imaging studies were performed within 2 wk from enrolment, and ADT is unlikely to have had a significant influence on the detectability of metastatic lesions [27]. Only five patients were having on-going ADT before imaging, and all these patients had high-volume metastatic disease detected by all imaging modalities.

An explicit strength of this study was the relatively high percentage of radical prostatectomies (28%), of which 77% were considered curative with undetectable 3-mo postoperative PSA levels. Our results provide additional information on the SUVmax level of PSMA-uptake foci found in these patients. Consequently, 10/17 curatively operated patients had low PSMA-uptake foci without anatomical correspondence in bone, all of whom were considered to have nonmalignant lesions, also having undetectable PSA levels after surgery. These low-to-moderate uptake bone foci lacking corresponding imaging findings are a challenge and necessitate caution when interpreting the nature of PSMA-positive lesions in bone, especially in the ribs [28].

A primary strength of our study is that all patients underwent all five imaging modalities, which were completed in a median of 8 d per patient. Furthermore, the study strengths included blinded double reading of all imaging modalities to define inter-reader variability and extended follow-up (median 435 d) supporting the imaged-based validation. Six patients were diagnosed with metastatic disease having only PSMA-positive lesions. All these lesions were considered malignant based on moderate-to-high PSMA uptake and anatomic correspondence found retrospectively with MRI and/or on follow-up imaging. Moreover, there were no PSMA-negative malignant bone lesions in this trial, although there is some evidence of low or even negative PSMA uptake in sclerotic bone metastases [29]. Several sclerotic bone lesions detected by CT (n = 30) were confirmed by WBMRI to represent nonmalignant aetiology.

We wish to emphasise that multicentre standardisation for SUVs with ^{18}F-PSMA-1007 tracer is a prerequisite for comparable results within and among participating clinics in future multicentre trials. The regularised PET image reconstruction algorithm (GE Healthcare, Milwaukee, WI, USA) used in the present trial may have improved lesion detectability and given higher SUV values than standard ordered subset expectation maximisation PET image reconstruction [30].

5. Conclusions

In summary, ^{18}F-PSMA-1007 PET-CT has superior sensitivity for detecting distant PCa metastases, but at the expense of false positive bone lesions. Keeping this in mind, PSMA PET-CT is a reliable tool for primary distant metastasis staging of high-risk PCa.

***Author contributions*:** Mikael Anttinen had full access to all the data in the study and takes responsibility for the integrity of the data and the accuracy of the data analysis.
Study concept and design: Anttinen, Boström, Seppänen, Aronen, Ettala, Saunavaara, Noponen.
Acquisition of data: Anttinen, Ettala, Malaspina, Timonen, Jambor, Rinta-Kiikka, Schildt, Rautio, Matikainen, Kajander.
Analysis and interpretation of data: Anttinen, Ettala, Malaspina, Seppänen, Löyttyniemi, Sandell, Boström.
Drafting of the manuscript: Anttinen, Seppänen, Boström, Taimen.
Critical revision of the manuscript for important intellectual content: Dean, Taimen, Boström, Blanco Sequeiros, Seppän.
Statistical analysis: Ettala, Löyttyniemi, Anttinen.
Obtaining funding: Boström, Aronen, Seppänen, Blanco Sequeiros.
Administrative, technical, or material support: Saukko, Saunavaara, Noponen, Aronen, Blanco Sequeiros, Seppänen.
Supervision: Boström, Seppänen, Aronen, Blanco Sequeiros, Kemppainen.
Other: None.

***Financial disclosures*:** Mikael Anttinen certifies that all conflicts of interest, including specific financial interests and relationships and affiliations relevant to the subject matter or materials discussed in the manuscript (eg, employment/affiliation, grants or funding, consultancies, honoraria, stock ownership or options, expert testimony, royalties, or patents filed, received, or pending), are the following: Dr. Anttinen reports grants from Profound Medical Inc., Finnish Urological Research Foundation and Finnish Urological Association, outside the submitted work. Dr. Ettala reports nonfinancial support from Ferring Pharmaceuticals Inc., SwanMedica, and Pierre-Fabre Pharma Norden AB; and personal fees from Astellas, outside the submitted work. Dr. Sandell reports personal fees from Roche, outside the submitted work. Dr. Taimen reports personal fees from Roche, AstraZeneca, and MSD; and nonfinancial support from MSD, all outside the submitted work. Dr. Boström reports grants from the Cancer Foundation Finland, and personal fees from Profound Medical Inc. and Janssen-Cilag Company, outside the submitted work. The other authors declare that there is no conflict of interest regarding the publication of this article.

***Funding/Support and role of the sponsor*:** financial support provided by Finnish Government Research and Development Fundsfor

Medical Research, Turku University Hospital, and TYKS-SAPA Research Fund.

Acknowledgements: We thank all the patients and referring physicians whose participation made this study project possible. We thank the entire staff team in the departments of Medical Physics, Diagnostic Radiology, Clinical Physiology, and Nuclear Medicine, and the Turku PET Centre at the Turku University Hospital. We want to also thank the staff team of the urological outpatient clinic at the Turku University Hospital, especially Sara Karnell, Kaisa Reunanen, and Tarja Lamminen, for their contribution to the project. Without their help and support, timely completion of this project could not have been accomplished.

Data sharing statement: All the data collected for this study, including the deidentified individual participant data, and the study protocol, statistical analysis plan, and informed consent form (in Finnish) will be available to anyone who wishes to access the data for a period commencing with publication and ending 5 yr later. Proposals for gaining access to the data should be directed to eliisa.loyttyniemi@utu.fi. Requestors will need to sign a data access agreement.

Appendix A. Supplementary data

Supplementary material related to this article can be found, in the online version, at doi:https://doi.org/10.1016/j.euo.2020.06.012.

References

[1] Welch HG, Gorski DH, Albertsen PC. Trends in metastatic breast and prostate cancer—lessons in cancer dynamics. N Engl J Med 2015;373:1685–7.
[2] Mottet N, Bellmunt J, Bolla M, et al. EAU-ESTRO-SIOG guidelines on prostate cancer. Part 1: screening, diagnosis, and local treatment with curative intent. Eur Urol 2017;71:618–29.
[3] Hövels A, Heesakkers R, Adang EM, et al. The diagnostic accuracy of CT and MRI in the staging of pelvic lymph nodes in patients with prostate cancer: a meta-analysis. Clin Radiol 2008;63:387–95.
[4] Suh CH, Shinagare AB, Westenfield AM, Ramaiya NH, Van den Abbeele AD, Kim KW. Yield of BS for the detection of metastatic disease in treatment-naive prostate cancer: a systematic review and meta-analysis. Clin Radiol 2018;73:158–67.
[5] Jambor I, Kuisma A, Ramadan S, et al. Prospective evaluation of planar BS, SPECT, SPECT/CT, 18F-NaF PET/CT and whole body 1.5 T MRI, including DWI, for the detection of bone metastases in high risk breast and prostate cancer patients: SKELETA clinical trial. Acta Oncol 2016;55:59–67.
[6] Perera M, Papa N, Roberts M, et al. Gallium-68 prostate-specific membrane antigen positron emission tomography in advanced prostate cancer-updated diagnostic utility, sensitivity, specificity, and distribution of prostate-specific membrane antigen-avid lesions: a systematic review and meta-analysis. Eur Urol 2020;77:403–17.
[7] Hofman MS, Lawrentschuk N, Francis RJ, et al. Prostate-specific membrane antigen PET-CT in patients with high-risk prostate cancer before curative-intent surgery or radiotherapy (proPSMA): a prospective, randomised, multi-centre study. Lancet 2020;395:1208–16.
[8] Thoeny HC, Froehlich JM, Triantafyllou M, et al. Metastases in normal-sized pelvic lymph nodes: detection with diffusion-weighted MR imaging. Radiology 2014;273:125–35.
[9] Komori T, Narabayashi I, Matsumura K, et al. 2-[Fluorine-18]-fluoro-2-deoxy-D-glucose positron emission tomography/computed tomography versus whole-body diffusion-weighted MRI for detection of malignant lesions: Initial experience. Ann Nucl Med 2007;21:209–15.
[10] Giesel FL, Will L, Lawal I, et al. Intraindividual comparison of 18F-PSMA-1007 and 18F-DCFPyL PET/CT in the prospective evaluation of patients with newly diagnosed prostate carcinoma: a pilot study. J Nucl Med 2018;59:1076–80.
[11] Cardinale J, Schäfer M, Benešová M, et al. Preclinical evaluation of 18F-PSMA-1007, a new prostate-specific membrane antigen ligand for prostate cancer imaging. J Nucl Med 2017;58:425–31.
[12] Kesch C, Kratochwil C, Mier W, Kopka K, Giesel FL. 68Ga or 18F for prostate cancer imaging? J Nucl Med 2017;58:687–8.
[13] Sheikhbahaei S, Werner AW, Solnes LB, et al. Prostate-specific membrane antigen (PSMA)-targeted PET imaging of prostate cancer: an update on important pitfalls. Semin Nucl Med 2019;49:255–70.
[14] Fendler WP, Eiber M, Beheshti M, et al. 68 Ga-PSMA PET/CT: Joint EANM and SNMMI procedure guideline for prostate cancer imaging: version 1.0. Eur J Nucl Med Mol Imaging 2017;44:1014–24.
[15] Harris PA, Taylor R, Minor BL, et al. The REDCap consortium: building an international community of software platform partners. J Biomed Inform 2019;95:103208.
[16] Lecouvet FE, Geukens D, Stainier A, et al. Magnetic resonance imaging of the axial skeleton for detecting bone metastases in patients with high-risk prostate cancer: diagnostic and cost-effectiveness and comparison with current detection strategies. J Clin Oncol 2007;25:3281–7.
[17] Lecouvet FE, El Mouedden J, Collette L, et al. Can whole-body magnetic resonance imaging with diffusion-weighted imaging replace Tc 99m bone scanning and computed tomography for single-step detection of metastases in patients with high-risk prostate cancer? Eur Urol 2012;62:68–75.
[18] Calais J, Ceci F, Eiber M, et al. 18F-fluciclovine PET-CT and 68Ga-PSMA-11 PET-CT in patients with early biochemical recurrence after prostatectomy: a prospective, single-centre, single-arm, comparative imaging trial. Lancet Oncol 2019;20:1286–94.
[19] Brierley JD, Gospodarowicz MK, Wittekind C. TNM classification of malignant tumours. John Wiley & Sons; 2017.
[20] Hanley JA, McNeil BJ. A method of comparing the areas under receiver operating characteristic curves derived from the same cases. Radiology 1983;148:839–43.
[21] Burdett S, Boeve LM, Ingleby FC, et al. Prostate radiotherapy for metastatic hormone-sensitive prostate cancer: a STOPCAP systematic review and meta-analysis. Eur Urol 2019;76:115–24.
[22] Lecouvet FE, Oprea-Lager DE, Liu Y, et al. Use of modern Imaging methods to facilitate trials of metastasis-directed therapy for oligometastatic disease in prostate cancer: a consensus recommendation from the EORTC Imaging Group. Lancet Oncol 2018;19:e534–45.
[23] Fanti S, Minozzi S, Antoch G, et al. Consensus on molecular imaging and theranostics in prostate cancer. Lancet Oncol 2018;19:e696–708.
[24] Phillips R, Shi WY, Deek M, et al. Outcomes of observation vs stereotactic ablative radiation for oligometastatic prostate cancer: the ORIOLE phase 2 randomized clinical trial. JAMA Oncol 2020;6:650–9.
[25] Roach PJ, Francis R, Emmett L, et al. The impact of 68Ga-PSMA PET/CT on management intent in prostate cancer: results of an Australian prospective multicenter study. J Nucl Med 2018;59:82–8.
[26] Fanti S, Lalumera E. Of standard of reference and accuracy: the problem of truth in imaging. Eur J Nucl Med Mol Imaging 2016;43:52–4.
[27] Ettala O, Malaspina S, Tuokkola T, et al. Prospective study on the effect of short-term androgen deprivation therapy on PSMA uptake evaluated with 68 ga-PSMA-11 PET/MRI in men with treat-

ment-naïve prostate cancer. Eur J Nucl Med Mol Imaging 2020;47:665–73.

[28] Zacho HD, Ravn S, Afshar-Oromieh A, Fledelius J, Ejlersen JA, Petersen LJ. Added value of 68Ga-PSMA PET/CT for the detection of bone metastases in patients with newly diagnosed prostate cancer and a previous 99mTc bone scintigraphy. EJNMMI Res 2020;10:31.

[29] Janssen J, Woythal N, Meißner S, et al. [68 Ga] PSMA-HBED-CC uptake in osteolytic, osteoblastic, and bone marrow metastases of prostate cancer patients. Mol Imaging Biol 2017;19:933–43.

[30] Lantos J, Mittra ES, Levin CS, et al. Standard OSEM vs. regularized PET image reconstruction: qualitative and quantitative comparison using phantom data and various clinical radiopharmaceuticals. Am J Nucl Med Mol Imaging 2018;8:110–8.